Physica Scripta T171 (2020) 014062

Influence of Plasma Heat Loads Relevant to ITER Transient Events on Deuterium Retention in Tungsten.

A.G. Poskakalov[1.2], Yu.M. Gasparyan[1], V.S. Efimov[1], D.V. Kovalenko[2], V.A. Barsuk[2], N.S. Klimov[1.2], M.S. Zibrov[3], O.V. Ogorodnikova[1]

1. National Research Nuclear University "MEPhI", Kashirskoe shosse, 31, 115409, Moscow, Russia
2. State Research Center of Russian Federation Troitsk Institute for Innovation and Fusion Research, ul. Pushkovykh, vladenie 12, 108840, Troitsk, Moscow, Russia.
3. Max Planck Institute for Plasma Physics, Boltzmannstrasse 2, 85748 Garching, Germany

E-mail: aposkakalov@gmail.com

Abstract. Deuterium (D) retention in Tungsten (W) under plasma heat loads relevant to edge localized modes in ITER was experimentally investigated at the QSPA-T plasma gun facility. Samples were exposed to 1.0 ms D plasma pulses with different heat loads in the range of 0.4–3.7 MJm^{-2} (heat flux factor $P\sqrt{t}$ = 13.3–123 $MJm^{-2}s^{-0.5}$). A significant D retention was observed already after one pulse. Moreover, the D retention grew up continuously with increasing the power load, although the surface was melted at highest loads (above 1.4 MJ/m^2). The D retention was higher than that in the case of stationary plasma irradiation at 600-700 K, indicating possible significant contribution of ELM's-like events to the total D retention. All stages of the experiments (irradiation, storage time and TDS) have been simulated using the TMAP 7 code.

Keywords: deuterium, retention, tungsten, nuclear fusion, high heat loads

Introduction

Tungsten (W) is a material for the divertor in ITER and is also considered for plasma facing components (PFCs) in future fusion devices. In addition to stationary high heat and particle fluxes, PFCs in fusion devices are exposed to enhanced pulsed fluxes during transient events, such as edge localized modes (ELMs) and thermal quench phases of disruptions. Damage of PFCs during transient events determines their lifetime [1]. Pulsed heat loads comparable to those of ITER ELMs and disruptions are difficult to achieve in the existing tokamaks given their smaller size and thus small stored energy. Therefore, other devices such as ion sources [2], electron-beam facilities [3], laser beams [4] and powerful plasma guns [5–7] are used to study the material behavior.

Previous studies performed at QSPA-T plasma gun (SRC RF TRINITI) [2] and the electron beam facility JUDITH (Forschungszentrum Jülich) [8], were focussed on macroscopic behaviour of tungsten PFCs. According to these investigations, the crack formation on the surface is the main damage process of tungsten PFCs under ITER-relevant ELM-like heat loads below the melting threshold of W. The melt layer movement and splashing are the main damage processes of W at the heat loads above the melting threshold.

In this work, deuterium (D) retention in W after plasma exposure in the QSPA-T facility was analyzed by thermal desorption spectroscopy (TDS) and the D depth profile were measured using nuclear reaction analysis (NRA). All stages of experiments (irradiation, storage time and TDS) have been simulated using the TMAP 7 code.

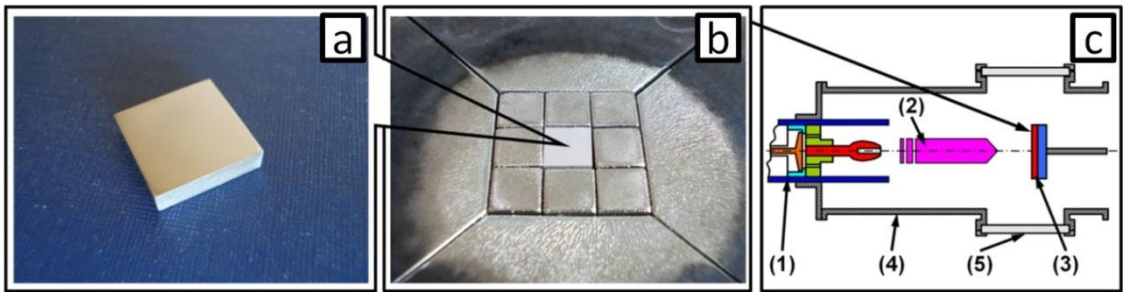

Figure 1. The scheme of the samples exposure at the QSPA-T facility: *a* — photo of the W sample before exposure; *b* — photo of the sample, which is mounted into the target; *c* — the scheme of the target exposure; (1) — the plasma gun; (2) — the plasma stream (D); (3) — the target; (4) — the target vacuum chamber; (5) — the diagnostics window.

Experimental details

The samples (10×10×2 mm^3) were cut from the sheet of rolled W (grade W-MP) with the density of 19.25 g/cm^3 [9]. It has a polycrystalline structure with the grain size of about 30 μm. The impurity content is below 0.05 wt.%. The plasma facing side (10×10 mm^2) of each sample was mechanically polished. For performing plasma exposures, each sample was surrounded by the following two parts to have a full-size (140×140 mm^2) target (figure 1*b*): (1) 8 identical samples surrounded the investigated sample to form the central area with the size of 34×34 mm^2; (2) the central area was surrounded by 4 Mo plates.

The general scheme of the target plasma exposure at the QSPA-T facility is presented in figure 1*c*. The exposed target (*3*) is placed in the vacuum chamber (*4*) at the distance of 40 cm from the plasma gun (*1*). The target center, where the sample is placed, was positioned in the plasma stream axis. In the present experiments, the plasma facing surface of the sample was oriented perpendicularly to the plasma stream (*2*).

Samples were exposed to D plasma. The initial energy of D particles leaving from the plasma source is below 1 keV. As a result of braking the plasma stream on the target the dense (up to $10^{23} m^{-3}$) and relatively cold plasma layer (<5 eV) forms near the target surface [10]. Therefore, it is considered that the average energy of particles bombarding the target is below 10 eV. The results of some previous experiments are described in [11 – 16]. The plasma stream duration t was 1.0 ms in all experiments. The plasma heat load q was varied in the range of 0.4–3.7 MJm^{-2} (the heat flux factor $P\sqrt{t}$ = 13.3–123 $MJm^{-2}s^{-0.5}$). The melting threshold of W (50 $MJm^{-2}s^{-0.5}$) is in the middle of this range [17]. The typical pulse waveform of 1.0 ms duration and its approximation by a trapezium pulse are presented in figure 2.

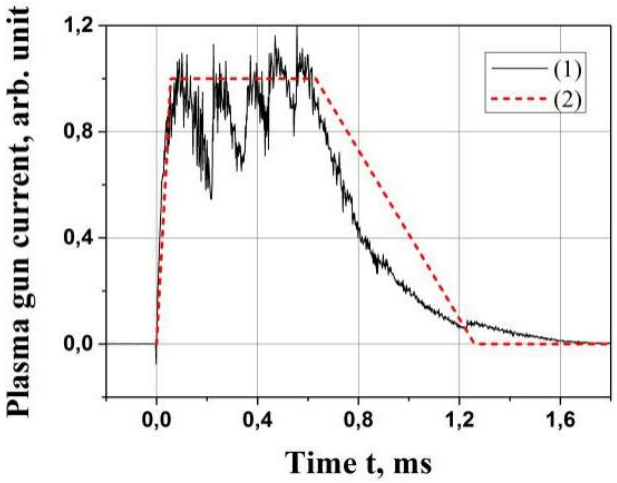

Figure 2. Typical pulse waveform: (1) — the measured plasma gun current during sample exposure; (2) — the trapezium approximation, which is used for calculation of the temperature and diffusion dynamics during exposure.

Each tungsten sample was exposed to a plasma stream with the fixed parameters by only one time and cooled down to the room temperature (RT) inside facility. There was no active cooling system and the samples were cooled only through lateral sides due to connection with neighbor elements of the target and due to radiation. The temperature of samples on the rear side during cooling down phases was measured by a chromel–alumel thermocouple.

The D retention in the samples was measured by means of thermal desorption spectroscopy in the UHV TDS facility [18]. The heating rate was 2 K/s. The desorption flux of all D containing molecules was monitored by the quadrupole mass spectrometer, which was calibrated after each experiment. Deuterium depth profiles in two samples exposed with heat loads below (0.7 MJ/m^2) and above (2.7 MJ/m^2) the W melting threshold, were measured using $D(^3He,p)\alpha$ nuclear reaction analysis (NRA) at the tandem accelerator (IPP, Garching). Six different ^3He energies varying from 0.69 MeV to 4.5 MeV were used to obtain data from different sample depths. D concentration profiles were obtained from the measured energy spectra of protons using SIMNRA and NRADC programs [19].

Experimental results

Figure 3 shows TDS spectra of the D_2 release from W, which was dominant in comparison to other D containing molecules. Deuterium is released in the temperature range from 600 K to 1300 K and the maximum of the spectrum increases with increasing the heat load (from 750 K to 1000 K). This suggests that D is released from deeper layers in the bulk and/or is trapped in defects with higher binding energies.

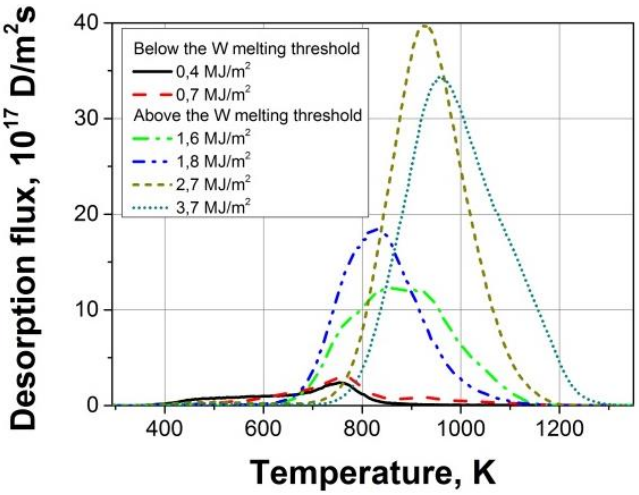

Figure 3. TDS of D_2 from W after exposure to one plasma pulse with the heat loads below and above the W melting threshold (1.4 MJ/m^2).

Deuterium depth profiles in W within the first 7 μm after the exposure to one pulse with the heat load below (0.7 MJ/m^2) and above (2.7 MJ/m^2) the W melting threshold are shown in figure 4. For low heat load irradiation, the D concentration is nearly constant at the level of 10^{-5} at fr. except first 40 nm, where the enhanced D concentration is observed. In the case of 2.7 MJ/m^2 irradiation, the D concentration is close to the background level in the first two microns and again at the level of about 10^{-5} at fr. behind this depth. According to SEM analysis of the cross-section of similarly exposed W samples in [20], the top layer with the thickness of about 2 μm has also a different structure with needle-shape crystals.

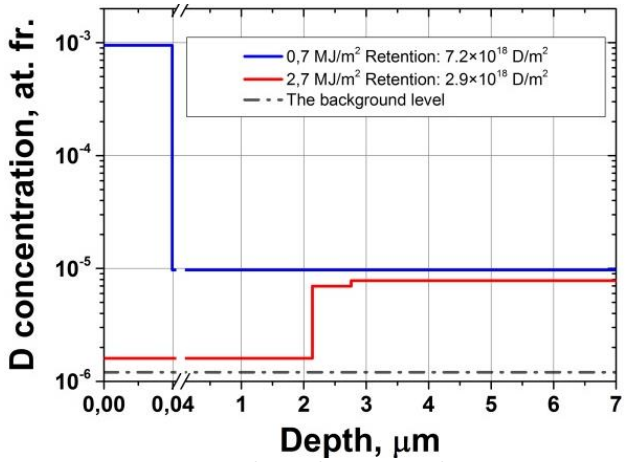

Figure 4. Depth profiles of D in W after exposure to one pulse of plasma gun with heat load above (2.7 MJ/m^2) and below (0.7 MJ/m^2) the W melting threshold and the D retention within first 7 μm.

Figure 5 shows the total D retention in W after different heat loads. Significant D retention was observed already after one pulse. It grows up continuously with increasing the heat load. The D retention is 2.59×10^{19} D/m^2 after irradiation with the heat load 0.4 MJ/m^2 and 4.1×10^{20} D/m^2 after 3.7 MJ/m^2 irradiation. The D retention in our experiments is higher than that in the case of stationary plasma irradiation [21] at 600-700 K, indicating possible significant contribution of ELM's-like events to the total D retention in fusion devices.

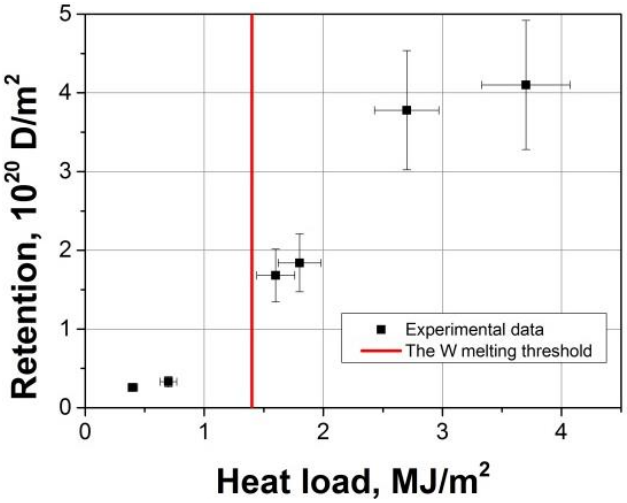

Figure 5. The D retention in W after exposure to one pulse of plasma gun with heat load above and below the W melting threshold.

Comparison of TDS and NRA shows that the main D retention occurs in deeply the bulk. The D retention within the first 7 μm is 7.2×10^{18} D/m^2 and the total D retention is 3.3×10^{19} D/m^2 under the heat load below the W melting threshold (0.7 MJ/m^2). In the case of the heat load above the W melting threshold (2.7 MJ/m^2), the D retention within the first 7 μm is 2.9×10^{18} D/m^2 and the total D retention is 3.8×10^{20} D/m^2. These data show that D is accumulated in W far away from the irradiated surface and the higher heat load is the higher is D migration in the bulk and the total retention. This can be explained by the very high temperature of the subsurface layer and a high temperature gradient during the plasma irradiation. Deuterium is weakly bounded in the subsurface layer under these conditions, but it can diffuse very quickly in the bulk and be trapped in colder regions.

Modeling in TMAP7

TMAP7 [22] numerically solves one dimensional equations for H diffusion, trapping and heat transport, taking into account surface recombination. Characteristics of the plasma stream and the plasma heat loads were taken from the results of previous experiments in the QSPA-T: Time dependences of heat and particle fluxes to the target were not directly measured, but they were assumed to be proportional to the trapezium shape shown in figure 2. Integral heat loads were calculated on the base of previous calibration experiments. The total fluence was assumed to be the same for all plasma exposures and was estimated on the base of the flow rate of the working gas in plasma source. The incident flux of D ions was estimated to be 7.5×10^{26} D /m^{2}s with the ion energy below 5 eV. For the simplicity, the modeling was made only for the heat loads below the melting threshold of W: 0.4 MJ/m^2, 0.7 MJ/m^2, 1.0 MJ/m^2, and 1.4 MJ/m^2 and the pulse duration of 1.0 ms. The Frauenfelder's value [23] for hydrogen diffusivity in W was used. The reported effective recombination rate coefficient on the W surface has a large scatter [24]. In this work, the recombination coefficient was taken according to the Pick and Sonnenberg's model [25] with the heat of H solution of E_s=1.04 eV [22] and the activation energy for chemisorption in the range of E_c = (0–1) eV. Temperature dependences of W thermal conductivity and volumetric heat capacity were taken according to [26].

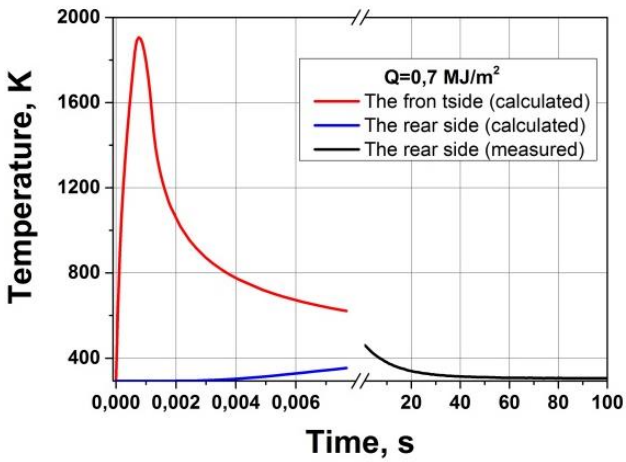

Figure 6. The experimental time dependence of the temperature on the rear side and the calculated temperature on the front surface in the case of head load of 0.7 MJ/m^2.

Realistic evolution of the sample temperature is important for the modeling. We were able to measure experimentally (with 1 sec resolution) only the dynamics of the temperature on the rear side of the sample during the cooling stage and it was used as an input parameter in the calculations, except 1 s after irradiation. The dynamics of the temperature during irradiation and in the first 1 s after irradiation was calculated in assumption of adiabatic conditions on both sides. According to calculations, the

temperature of both sides is nearly equal at this time. Further dynamics of the temperature dynamics was calculated using the experimental data on the rear side and adiabatic conditions on the front side. Figure 6 presents the example of the temperature dynamics in the case of 0.7 MJ/m^2 irradiation.

The sample with the heat load of 0.7 MJ/m^2 was the most characterized, therefore, we performed most of analysis for this experiment. The choice of the trapping concentration was based on NRA data. We ignored an increased D concentration in the first 40 nm to simplify the modeling and due to low contribution of this part to the total D retention. Modeling using the uniform trap distribution with various concentrations in the range of 10^{-5}–10^{-2} at. fr. and the detrapping energy of 1.5 eV is presented in figure 7. The storage time after irradiation was 10000 seconds in all calculations. Most significant changes in D depth distribution stopped already till this time, that is, however, much less than in real experiments.

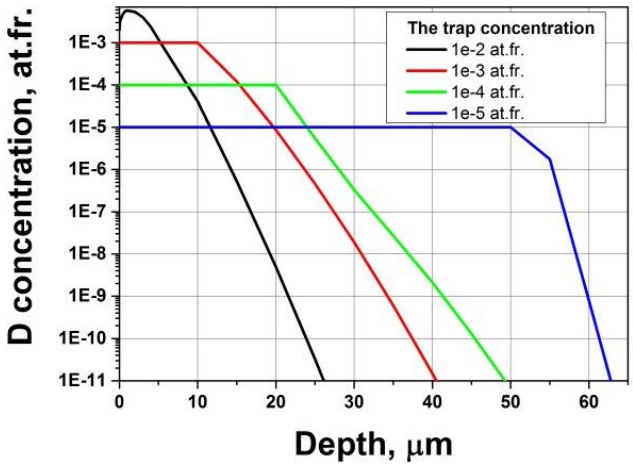

Figure 7. Calculated depth profiles of D in W after exposure to one pulse of the plasma gun with the different trap concentration (10000 sec after irradiation, the detrapping energy – 1.5 eV).

The population of traps by D in the surface layer was usually small just after irradiation. However, nearly 100% population of traps was observed in the first 7 μm at the end of the storage time. This is due to transport of solute D atoms to the surface from the bulk with subsequent trapping. Similar results were obtained also for the detrapping energy of 1.0 eV. Since the D concentration was measured to be 10^{-5} at.fr., the trap concentration of 10^{-5} at.fr. was used further.

Figure 8 shows the influence of the detrapping energy on calculated TDS spectra. Using the uniform trap distribution, the best agreement with the experiment was achieved in the case of 1.5 eV traps, that is typical for the vacancies in W [27, 28]. The calculated spectrum for the energy of 1.0 eV (close to the value for dislocations [27]) is also given for comparison.

The experimental TDS spectrum in fig.8 has two peaks in contrast to the calculated one, that can be due to additional type of traps or more complicated trap distribution in the bulk.

The additional free parameter in calculations is the surface recombination coefficient. Strong influence of the choice of the recombination coefficient on the results was observed. This is usually not the case at low irradiation temperatures [29], but at very high surface temperatures like in QSPA-T, Pick-Sonnenberg's model predicts a strong decrease of the recombination coefficient, and therefore, the effect is large.

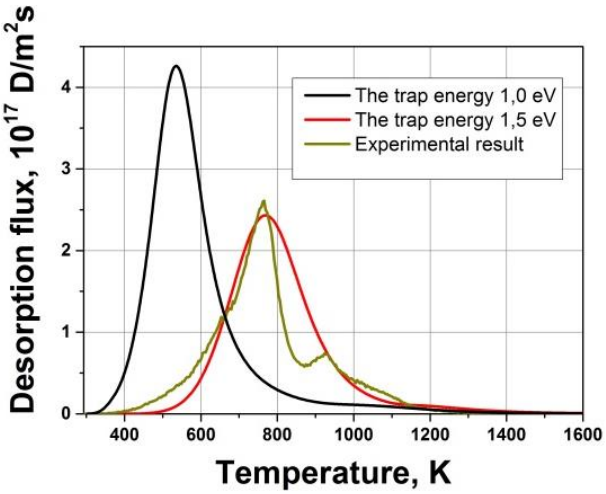

Figure 8. Comparison of the experimental and calculated TDS data for the heat load of 0.7 MJ/m^2 (10000 sec after irradiation, the detrapping energies are 1.0 and 1.5 eV).

Figure 9 compares calculated values of the total D retention in W samples after QSPA-T plasma pulses with various heat loads using two different activation energy in the recombination coefficient: -2.06 eV (zero surface barrier) and -0.2 eV (E_c =0.93 eV). One can see much better agreement with two experimental points in the case of the non-zero surface barrier, therefore, this value was used in all results presented above (fig.7-8).

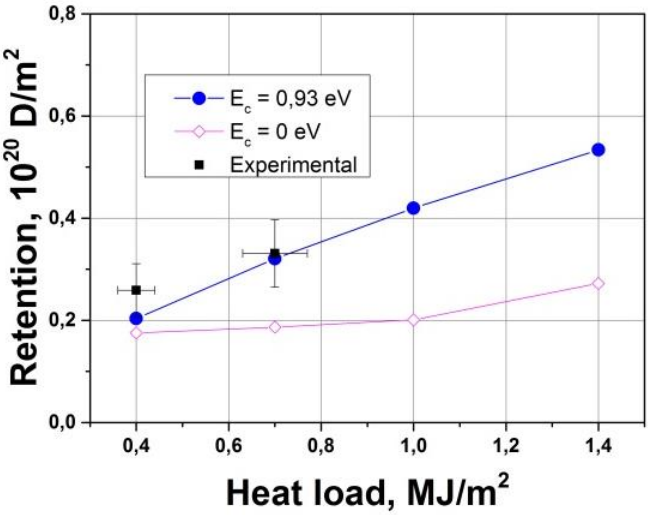

Figure 9. The calculated D retention in W after exposure to one pulse of the plasma gun with the heat load below the W melting threshold.

Thus, the reasonable agreement with the current experimental data below the melting threshold is obtained. Additional experiments with variation of the pulse duration and heat loads will be done in near future to perform more detailed calculations.

Summary

The D retention in W under plasma heat loads relevant to ITER edge localized modes was experimentally investigated in the QSPA-T plasma gun facility. Significant D retention was observed by TDS already after one pulse. Moreover, the D retention grew up continuously with increasing the heat load. In contrast to TDS, the D retention within the first 7 μm was rather small according to NRA measurements that are the indication of deep penetration of implanted D particles.

Simulations using the TMAP7 code demonstrated that deep D penetration into the bulk of W far away from the irradiated surface is indeed possible. Reasonable agreement with the experimental data below the melting threshold was possible to achieve using typical parameters for H in W.

Acknowledgement

This work was supported by the Russian Foundation for Basic Research (grant 18-32-20114\18).

References

[1] Loarte A *et al*. 2007 *Phys. Scripta* **T128** 222.
[2] Compan J *et al.* 2007 *Phys. Scripta* **T128** 246
[3] Linke J *et al*. 1994 *J. Nucl. Mater*. **212–215** 1195
[4]Huber A *et al.* 2013 *Fusion Science and Technology* **63 (1T)** 197–200
[5] Arkhipov N I *et al.* 2000 *Fusion Eng. Des.* **49–50** 151
[6] Tereshin V I *et al.* 2007 *Plasma Phys. Control. Fusion* **49** A231
[7] Zhitlukhin A *et al.* 2007 *J. Nucl. Mater*. **363–365** 301
[8] Pintsuk G. *et al.* 2015 *Fusion Engineering and Design*, **98—99** 1384
[9] http://www.polema.net/
[10] V.G. Belan *et al.* 1996 *J. Nucl. Mater*. **233-237** 763
[11] Klimov N *et al.* 2011 *Phys. Scripta* **T145** 014064
[12] Klimov N *et al.* 2009 J. Nucl. Mater. **390–391** 721
[13] Klimov N *et al.* 2011 *J. Nucl. Mater*. **415** S59
[14] Kovalenko D V *et al.* 2011 *Phys. Scr.* **T145** 014065
[15] Kuprianov I B *et al.* 2011 *Phys. Scr.* **T145** 014063
[16] Klimov N S *et al.* 2014 *Fusion Science and Technology* **V.66 (#1)** 118 – 124
[17] R.A. Pitts *et al.* 2013 *J. Nucl. Mater*. **438** 48
[18] Rusinov A A *et al.* 2009 *Instruments and Experimental Techniques*, **52** 871.
[19] K. Schmid, U. von Toussaint, 2012 *Nuclear Instruments and Methods in Physics Research Section B: Beam Interactions with Materials and Atoms*, **281** 64.
[20] Poskakalov A *et al.* 2018 *Problems of Atomic Science and Technology, Series Thermonuclear Fusion.* **41 (1)** 23
[21] Ogorodnikova O V *et al*. 2019 *J. Nucl. Mater.* **515** 150
[22] Longhurst G **2008** TMAP7 User Manual, INEEL/EXT-04–02352 Rev. 2
[23] Frauenfelder *R J* 1696 *Vac. Sci. Technol.* **6** 388
[24] Ogorodnikova O V 2019 *J. Nucl. Mater*. **522** 74
[25] Pick M A *1985 J. Nucl. Mater*. **131**, 208
[26] ITER Materials Properties Handbook
[27] Ogorodnikova O V 2015 *Journal of Applied Physics* **112** 074902
[28] M. Zibrov et al. **2016** *Journal of Nuclear Materials* **477** 292
[29] Roth J., Schmid K. 2011 *Phys. Scr.* **T145** 014031